Inorganic Chemistry

Article

pubs.acs.org/IC

^{95}Mo Solid-State Nuclear Magnetic Resonance Spectroscopy and Quantum Simulations: Synergetic Tools for the Study of Molybdenum Cluster Materials

Jérôme Cuny,*[,†,‡] Stéphane Cordier,[†] Christiane Perrin,[†] Chris J. Pickard,[§] Laurent Delevoye,*[,⊥] Julien Trébosc,[⊥] Zhehong Gan,[¶] Laurent Le Pollès,[†] and Régis Gautier*[,†]

[†]Institut des Sciences Chimiques de Rennes, UMR 6226, CNRS - Université de Rennes 1 - Ecole Nationale Supérieure de Chimie de Rennes, Avenue du Général Leclerc, CS 50837, 35708 Rennes Cedex 7, France

[§]Department of Physics & Astronomy, University College London, Gower Street, London WC1E 6BT, U.K.

[⊥]Unité de Catalyse et Chimie du Solide, UMR 8181, CNRS - Université de Lille 1, 59655 Villeneuve d'Ascq, France

[¶]National High Magnetic Field Laboratory, 1800 E. Paul Dirac Drive, Tallahassee, Florida 32310, United States

Supporting Information

ABSTRACT: The ability of ^{95}Mo solid-state nuclear magnetic resonance (SSNMR) spectroscopy to probe the atomic and electronic structures of inorganic molybdenum cluster materials has been demonstrated for the first time. Six cluster compounds were studied: $MoBr_2$, $Cs_2Mo_6Br_{14}$, $(Bu_4N)_2Mo_6Br_{14}$, each containing the octahedral $Mo_6Br_{14}^{2-}$ cluster unit, and MoS_2Cl_3, $Mo_3S_7Cl_4$, and MoSCl that contain metallic dimers, trimers, and tetramers, respectively. To overcome inherent difficulties due to the low sensitivity of ^{95}Mo SSNMR, both high-magnetic-field spectrometers and the quadrupolar Carr−Purcell Meiboom−Gill sensitivity enhancement pulse sequence under magic-angle-spinning conditions, combined with a hyperbolic-secant pulse were used. Experimental measurements as well as characterization of the ^{95}Mo electric field gradient and chemical shift tensors have been performed with the help of quantum-chemical calculations under periodic boundary conditions using the projector augmented-wave and the gauge-including projector augmented-wave methods, respectively. A large ^{95}Mo chemical shift range is measured, ∼3150 ppm, and the isotropic chemical shift of the Mo atoms is clearly correlated to their formal oxidation degree in the various clusters. Furthermore, a direct relation is evidenced between the molybdenum quadrupolar coupling constant and the bond lengths with its surrounding ligands. Our results demonstrate the efficiency of the combined use of quantum-chemical calculations and ^{95}Mo SSNMR experiments to study inorganic molybdenum cluster compounds.

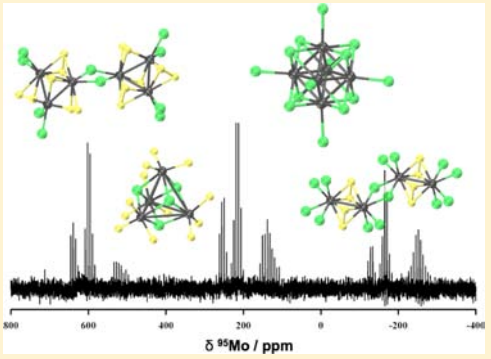

INTRODUCTION

Among the promising developments in materials science, metal cluster compounds have been the subject of increasing interest for the last 10 years. As defined by Cotton, these clusters are metallic aggregates that exhibit different nuclearities, wherein metal atoms are directly connected by metal−metal bonds.[1] The number of electrons involved in these metal−metal bonds, often called the valence electron count, influences the general properties of the aggregates. In particular, their delocalization on the whole cluster leads to a wide range of specific physical properties such as luminescence[2] and molecular magnetism[3,4] that are of interest in different application areas. The metallic core is generally covalently bonded to face-capping or edge-bridged ligands (L^i, where i stands for inner) and stabilized by terminal ligands (L^a, where a stands for apical), yielding a so-called cluster unit. These species, which can be discrete or condensed by either ligands or metals, constitute the basic building blocks of a wide range of inorganic, hybrid organic−inorganic, and supported materials and nanomaterials that can be prepared by either solid-state or solution chemistry.[5]

Among the various families of metal clusters that encompass 3d, 4d, and 5d elements, inorganic molybdenum cluster compounds present one of the most interesting and richest crystallochemistries in terms of the diversity and complexity of structural edifices.[6,7] Indeed, a very large number of nuclearities and geometries are encountered, from the simplest cluster made of triply bonded pairs of Mo atoms found in $LaR_4Mo_{36}O_{52}$[8] to infinite chains of face-sharing octahedral clusters found in $Tl_2Mo_6Se_6$.[9,10] Between these two compounds, a number of intermediate geometries and nuclearities are found, many of them exhibiting original properties. For example, trinuclear Mo_3 clusters associated with dithiolene ligands have a great potential for the development of molecular

Received: July 27, 2012
Published: December 28, 2012

conductors.[11] The tetrahedral geometry of the Mo_4 cluster favors the formation of both clathrate frameworks with giant cells[12] and spinel-related structures having a Mott insulator behavior.[13] The latter exhibit an electric-field-induced resistive switching that is actually studied for the design of a new generation of resistive random access memory. The octahedral Mo_6 cluster constitutes the most encountered aggregate among the families of molybdenum clusters. Molecular compounds based on noninteracting $Mo_6X_{14}^{2-}$ cluster units (X = halogen) are characterized by insulating behavior combined with phosphorescent properties. Indeed, they absorb from ultraviolet to visible and emit on a wide optical window that ranges from visible to near-IR with high quantum yields and lifetimes.[14] The three-dimensional condensation of Mo_6 cluster units via ligands yields the superconducting Sergent−Chevrel phases,[15] whereas a one-dimensional condensation yields the semiconducting $Mo_6X_8Y_2$ compounds (X = halogen and Y = chalcogen).[16] The latter, used as a precursor for the elaboration of MoS_2 nanotubes and MoO_{3-x} nanowires,[17,18] are structurally similar to a new class of nanowire materials that was discovered 10 years ago and that is also based on a one-dimensional arrangement of octahedral clusters.[19,20] Among others, they exhibit interesting optical and tribological properties,[21−24] and are easily dispersed in organic solvents.[25−27] In selenium chemistry, the Mo_6 clusters generally condense through the sharing of triangular metallic faces, leading, for example, to the $Ag_{\sim 3.8}Mo_9Se_{11}$ compound based on Mo_9 clusters.[28] It exhibits a ZT value roughly equal to 0.7 at 800 K and is thus considered as the first member of a new category of promising thermoelectrics. The limit phase in this condensation process is reached in $Tl_2Mo_6Se_6$, which can be depicted as a molybdenum nanowire bonded to a matrix of Se atoms.[29] This compound is metallic with a superconducting transition at low temperature that makes it a relevant material cathode for the design of magnesium storage batteries.

In the aforementioned solid-state materials, the cluster unit is used as the basic entity enabling the description of crystal and electronic structures. It turns out that their dissolution leads to discrete units in solution that can be used in the elaboration of molecular assemblies and nanomaterials.[30] For example, the $Mo_6Br_{14}^{2-}$ cluster unit can be incorporated without modification into silica nanoparticles for bioimagery, biolabeling, or photonic application purposes[31,32] and in a polymer matrix as an oxygen sensor,[33,34] and it can be adsorbed on ZnO surfaces to form tunable visible-emitting particles.[35] More specifically, the fluorinated cluster unit $[Mo_6Br^i_8F^a_6]^{2-}$ has been incorporated in the MIL-101 zeolite to improve its hydrogen storage performances at room temperature from 1.2 to 4.8 $g{\cdot}cm^{-3}$.[36] The grafting of functional ligands on the cluster in solution yields original molecular assemblies, including dendrimers, that can be subsequently involved in the elaboration of hybrid nanocomposites.[37−43] In particular, functionalization by polymerizable ligands allows them to be dispersed in an organic matrix without phase segregation,[44] whereas functionalization by mesogenic ligands yields hybrid assemblies that can autoorganize to form liquid-crystal materials.[45,46] A similar observation has been made for $Tl_2Mo_6Se_6$, which, once dissolved in dimethylformamide, presents lyotropic liquid-crystal properties.[47] Finally, it has been shown that immobilization of octahedral clusters on silicon surfaces leads to the original molecular junction.[48,49]

^{95}Mo solid-state nuclear magnetic resonance (SSNMR) is a prime method for the structural characterization of these molybdenum cluster materials because most of their properties are directly linked to their metallic core and its local environment. This is all the more true in the case of amorphous or disordered materials such as nanoparticles, functionalized polymers, and surfaces for which the structural insights provided by X-ray diffraction techniques are limited. The number of difficulties often encountered in SSNMR of transition elements have been progressively overcome because of the technical progresses and developments of new pulse sequences. This enabled to study nuclei possessing unfavorable NMR properties such as ^{99}Ru,[50] ^{45}Sc,[51] ^{139}La,[52,53] ^{63}Cu, and ^{65}Cu.[54] However, among these unfavorable nuclei, Mo SSNMR is still poorly explored compared to the large range of applications of molybdenum compounds. Despite the existence of two NMR-active isotopes, ^{95}Mo and ^{97}Mo, the difficulty of Mo SSNMR is explained by their low natural abundance NA(^{95}Mo) = 15.72% and NA(^{97}Mo) = 9.46% and their low gyromagnetic ratios, $\gamma(^{95}\text{Mo}) = -1.751 \times 10^7$ $rad{\cdot}s^{-1}{\cdot}T^{-1}$ and $\gamma(^{97}\text{Mo}) = -1.788 \times 10^7$ $rad{\cdot}s^{-1}{\cdot}T^{-1}$. Furthermore, they are both quadrupolar nuclei of spin $^5/_2$ with quadrupole moments of $Q(^{95}\text{Mo}) = -22$ mB and $Q(^{97}\text{Mo}) = -255$ mB. The ^{95}Mo nucleus is generally preferred to ^{97}Mo because its lower quadrupolar moment allows one to achieve a higher resolution of the central transition powder patterns.[55]

Difficulties of ^{95}Mo SSNMR are underlined by the few available results. Since the first work of Lynch and Segel in 1972,[56] about 35 papers dealing with experimental ^{95}Mo SSNMR in both amorphous and crystallized compounds have been published.[57−91] This is not much compared to the large quantity of results published in the liquid state. Indeed, the review published 15 years ago by Malito even then included more than 500 molecules that represent a large and representative database of ^{95}Mo NMR isotropic chemical shift (CS) for each of the molybdenum oxidation states.[92] Apart from amorphous and supported materials,[57−67] the various studies encompass a set of about 55 crystalline compounds, where 48 are diamagnetic insulators. Among them, 42 are molybdates and polyoxomolybdates with fully oxidized or mixed-valence (V+ and VI+) Mo atoms in tetrahedral or octahedral oxygen environments. The 0 (four compounds) and IV+ (five compounds) oxidation states were also studied, among which is the molybdenite MoS_2, which has important industrial applications as a solid lubricant. The other materials are metallic and include the three molybdenum cluster compounds ever studied by ^{95}Mo SSNMR: Mo_6Se_8, Mo_6Te_8, and $LaMo_6Se_8$.[83−86] So far, no work on diamagnetic insulating molybdenum cluster compounds has been published. The total solid-state ^{95}Mo CS range is about 8000 ppm, ranging from +5885 ppm for molybdenum metal to −2100 ppm for $MoSi_2$.[83,84] If only insulating diamagnetic compounds are taken into account, this range is reduced from −1885 ppm for the tricarbonyl(mesitylene)molybdenum to +2181 ppm for $(NH_4)_2MoS_4$.[67,70] To our knowledge, only 14 publications deal with determination of the ^{95}Mo chemical shift anisotropy (CSA) parameters[62,64,66−74,80,90,91] and only one with the absolute orientation of the CS and electric field gradient (EFG) tensors.[69] Maximum values of 1010/1018 ppm (±5) and 7.8 MHz have been observed for the ^{95}Mo CSA and quadrupolar coupling constant in MoS_2 and MoO_2, respectively.[67,91]

A full interpretation of the SSNMR spectra, i.e., an accurate determination of both CS and EFG tensors, often remains a challenging task. This is especially true for low-γ nuclei, among which is ^{95}Mo, where a few experimental data on model

compounds are available. The use of first-principles calculations allows us to partially overcome these difficulties.[93] Like other available formalisms,[94−96] the projector augmented-wave (PAW) and gauge-including projector augmented-wave (GIPAW) methods are especially devoted to solid-state compounds because they explicitly take into account the periodicity of the systems.[97,98] They have already demonstrated their ability to accurately calculate the CS and EFG tensors of various elements, although very few studies have been devoted to transition-metal nuclei.[99] Their applications encompass a variety of chemical systems such as silicates, phosphates, various inorganic materials, organic crystals, carbon nanotubes, and other materials that are described in the review by Charpentier.[99] In most cases, these theoretical studies have been performed together with experimental measurements.

To be able, in the near future, to characterize complex molybdenum cluster materials by ^{95}Mo SSNMR, it is necessary to first gather preliminary information by studying a range of crystallized cluster compounds with well-defined crystalline structures. To achieve such a purpose, this paper presents the first combined experimental and theoretical study of six insulating diamagnetic cluster materials by ^{95}Mo SSNMR: $MoBr_2$,[100] $(Bu_4N)_2Mo_6Br_{14}$,[101] and $Cs_2Mo_6Br_{14}$,[102] each containing the octahedral $Mo_6Br_{14}^{2-}$ cluster, and MoS_2Cl_3,[103] $Mo_3S_7Cl_4$,[103] and MoSCl,[104] which contain the $Mo_2(S_2)_2Cl_8$ dimer, $Mo_3(S_2)_3SCl_6$ trimer, and $Mo_4S_4Cl_{12}$ tetramer, respectively. These compounds have been chosen because they cover a large range of oxidation states of molybdenum, i.e., II+ in $MoBr_2$, $(Bu_4N)_2Mo_6Br_{14}$ and $Cs_2Mo_6Br_{14}$, III+ in MoSCl, IV+ in $Mo_3S_7Cl_4$, and V+ in MoS_2Cl_3, and because the corresponding cluster units are the building block of more complex hybrid and nanomaterials. Thus, this makes the present study a valuable introduction for the future ^{95}Mo SSNMR characterization of these complex materials. As the availability of the experimental facilities was limited, our goal has been to optimize both the signal-to-noise ratio of our spectra and the amount of extractable information by benefiting from the use of a high-magnetic-field spectrometer associated with the quadrupolar Carr−Purcell-Meiboom−Gill (QCPMG) pulse sequence under magic-angle-spinning (MAS) conditions.[105−107] We have subsequently focused our analysis of the experimental data on the isotropic CS and, when possible, on the quadrupolar coupling parameters.

EXPERIMENTAL SECTION

Materials. $MoBr_2$, $(Bu_4N)_2Mo_6Br_{14}$, $Cs_2Mo_6Br_{14}$, $Mo_3S_7Cl_4$, and MoSCl have been prepared according to the methods described in the literature.[100−104] MoS_2Cl_3 was synthesized using a protocol slightly modified from the published one, allowing better control of the final composition.[103] The purity of the samples was tested by powder X-ray diffraction analysis using an INEL CPS 120 diffractometer equipped with a spatial localization curve detector. After X-ray analysis, each compound was sealed under vacuum and then was opened only to perform the NMR measurements. X-ray analysis was also performed after the NMR measurements and did not reveal any evolution of the samples.

SSNMR Spectroscopy. ^{95}Mo SSNMR experiments were conducted at the University of Lille 1 on a Bruker standard-bore Ultra-Stabilized 800 spectrometer operating at 18.8 T [$\omega_0(^{95}Mo)$ = 52.14 MHz] equipped with a 3.2 mm HX MAS probe and driven by an Avance II 800 console. The spinning rate was set to 20 kHz for all experiments. The magic angle was primarily tuned by visually maximizing the intensity of the spinning sidebands on a ^{2}H MAS NMR spectrum of a deuterated poly(methyl methacrylate) sample. The molybdenum CS was referenced to a 2.0 M aqueous solution of Na_2MoO_4 (δ_{iso} = 0 ppm). The descriptions of the two different pulse sequences used in this spectrometer, single-pulse and QCPMG-pulse sequences, are given in the Supporting Information. For $MoBr_2$, $(Bu_4N)_2Mo_6Br_{14}$, and $Cs_2Mo_6Br_{14}$, experiments were also conducted at the National High Magnetic Field Laboratory of Tallahassee, FL, using an ultranarrow-bore spectrometer equipped with a Magnex magnet operating at 19.6 T [$\omega_0(^{95}Mo)$ = 54.29 MHz]. The single-channel broad-band 7 mm MAS probe used in this case was optimized for the study of low-γ nuclei. A QCPMG pulse sequence under 5 kHz MAS conditions was used. This sequence is described in the Supporting Information.

All experiments were conducted under MAS conditions. For the measurements performed at a spinning rate of 20 kHz, we suppose that the CSA parameters have no influence on the shape of the observed spectra. We thus do not include them in the simulations presented in this paper (see the Supporting Information for simulations of the MoS_2Cl_3 and $Mo_3S_7Cl_4$ spectra including various sets of CSA parameters). For the three experiments performed at 5 kHz, our density functional theory (DFT) calculations suggest that the CSA parameters of the corresponding compounds are lower than 110 ppm. Consequently, we also neglect the CSA parameters during analysis of the corresponding spectra. The experimental NMR parameters C_Q, η_Q, and δ_{iso} were extracted from the QCPMG spectra by performing numerical simulations using the software *SIMPSON*, version 1.1.0.[108] A total of 4180 crystallite orientations were used to simulate the powder averaging. This number allows us to visually converge the shape of the simulated spectra. The experimental uncertainty of each NMR parameter was evaluated by a visual comparison between the experimental and simulated spectra. To do so, each parameter was varied bidirectionally, with all others being kept constant, until the shape variation was significant. Analytical simulations of the single-impulsion spectra were performed using the *Dmfit* software.[109]

DFT Calculations. All calculations were carried out using the *CASTEP 4.3* DFT code that explicitly describes the crystalline structure of the compounds using periodic boundary conditions.[110] The exchange-correlation interaction was described within the generalized gradient approximation (GGA) of Perdew, Burke, and Ernzerhof.[111] The valence-core interactions were described using ultrasoft pseudopotentials, which are described in the Supporting Information. The GIPAW and PAW formalisms were used to calculate the chemical shielding and EFG tensors, respectively, from the pseudodensity.[97,98,112,113] A set of convergence test calculations with energy cutoff values ranging from 400 to 600 eV were performed by a step of 50 eV. All of the ^{95}Mo NMR parameters were proven to converge with an energy cutoff of 500 eV. The Monkhorst−Pack *k*-point grid density used for each compound was tested from 2 × 2 × 2 to 6 × 6 × 6 and fully converged (see the Supporting Information).[114]

The calculated chemical shielding parameters σ_{iso}, σ_{aniso}, and η_σ are defined from the chemical shielding tensor eigenvalues by $\sigma_{iso} = (\sigma_{xx} + \sigma_{yy} + \sigma_{zz})/3$, $\sigma_{aniso} = \sigma_{zz} - \sigma_{iso}$, and $\eta_\sigma = (\sigma_{yy} - \sigma_{xx})/\sigma_{aniso}$ with $|\sigma_{zz} - \sigma_{iso}| \geq |\sigma_{xx} - \sigma_{iso}| \geq |\sigma_{yy} - \sigma_{iso}|$. These parameters can be transformed into the CS formulation using the general relation $\delta_{ij} = \sigma_{ref} - \sigma_{ij}$, where σ_{ref} is the isotropic chemical shielding of a reference compound. Because GIPAW calculations and experiments give access to the chemical shielding and CS tensors, respectively, a perfect correlation between the calculated and experimental isotropic values is obtained when $\delta_{iso}^{exp} = \sigma_{ref} - \sigma_{iso}^{calc}$. In that case, σ_{ref} is equal to the isotropic shielding of the experimental reference. When large CS ranges are considered, one generally deviates from this ideal case and the correlation more likely looks like $\delta_{iso}^{exp} = a[\sigma_{ref} - \sigma_{iso}^{calc}]$, where a described the quality of the correlation. The EFG tensor is traceless; i.e., its eigenvalues (V_{xx}, V_{yy}, and V_{zz}) obey $V_{xx} + V_{yy} + V_{zz} = 0$. We used the following conventions for the quadrupolar coupling constant C_Q and the asymmetry parameter η_Q: $C_Q = eQV_{zz}/h$ and $\eta_Q = (V_{xx} - V_{yy})/V_{zz}$ with $|V_{zz}| \geq |V_{xx}| \geq |V_{yy}|$. A quadrupolar moment Q for ^{95}Mo equal to −22 mb was used.[55,115] Because NMR experiments are not sensitive to the sign of Q at ambient temperature, all calculated and experimental C_Q values are set positive.

dx.doi.org/10.1021/ic301648s | *Inorg. Chem.* 2013, 52, 617−627

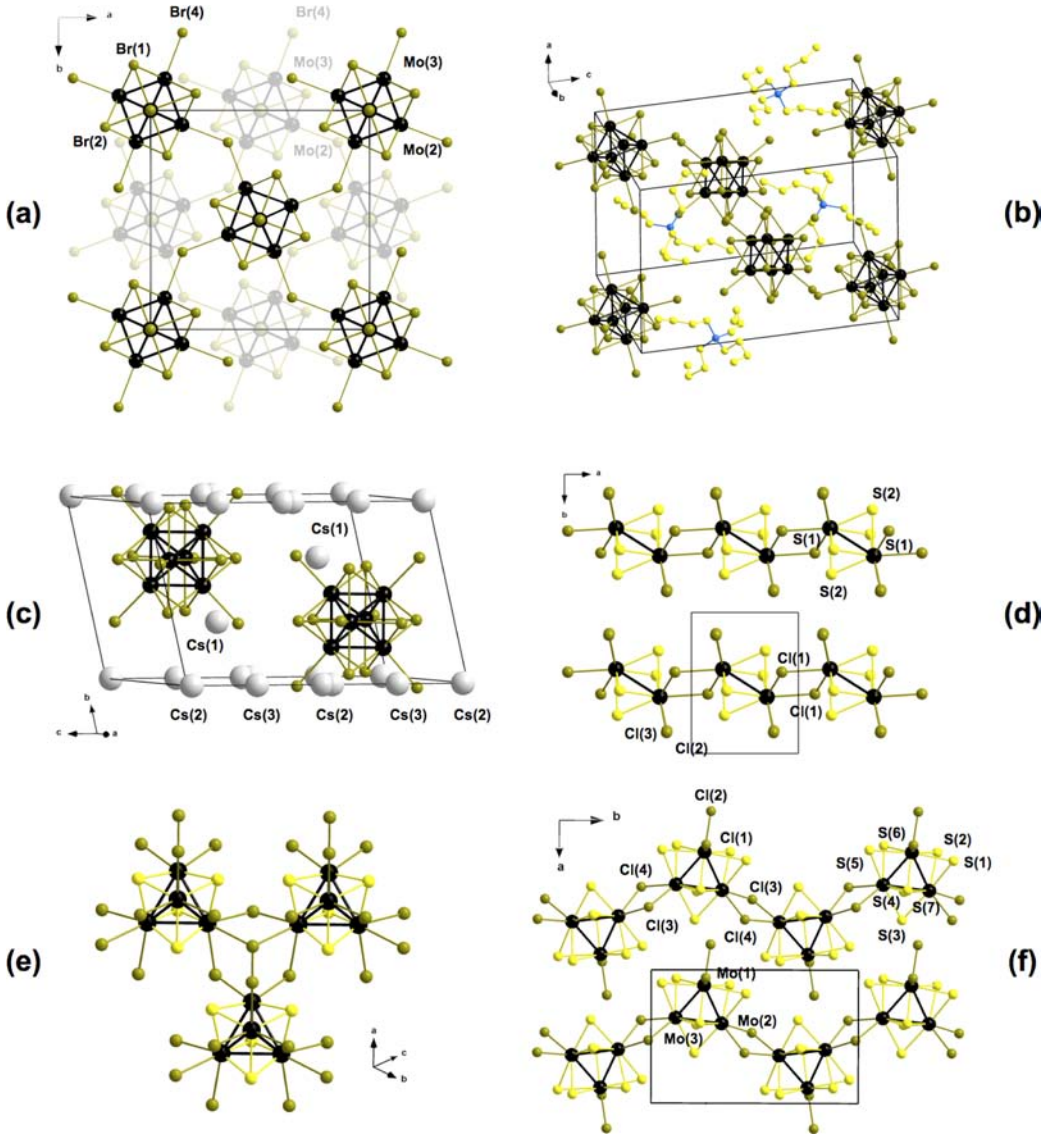

Figure 1. Crystallographic structures of the studied molybdenum cluster compounds. (a) View along the [001] direction of the $MoBr_2$ structure. The opaque atoms belong to the B plane of the A−B−A stacking scheme. Mo(1) and Br(3) are perpendicular to the *ab* plane. (b) Representation of the $(Bu_4N)_2Mo_6Br_{14}$ structure determined at 293 K. H atoms are not represented for clarity. (c) Representation of the $Cs_2Mo_6Br_{14}$ structure. All Cs positions are shown. (d) View along the [001] direction of the MoS_2Cl_3 structure. (e) Representation of the MoSCl structure. (f) Representation of the $Mo_3S_7Cl_4$ structure. The Mo, Br/Cl/N, Cs, and C/S atoms are represented by black, dark-gray, light-gray, and small white spheres, respectively.

It has been demonstrated that performing geometry optimizations can have a significant influence on the calculated NMR parameters.[116] Because the cell parameters are the crystallographic data that are determined with the best accuracy, only atomic positions were relaxed for computational efficiency. In the following, we only discuss the results obtained from these optimized structures. Details are provided in the Supporting Information.

RESULTS AND DISCUSSION

The crystal structures of the six studied compounds are depicted in Figure 1. In $Cs_2Mo_6Br_{14}$ and $(Bu_4N)_2Mo_6Br_{14}$, the clusters are isolated from one another because they do not share any halogen ligand. In all other compounds, halogen atoms are shared between different clusters. The different ligand-sharing modes give rise to monodimensional structures for MoS_2Cl_3 and $Mo_3S_7Cl_4$, a planar structure for $MoBr_2$, and a tridimensional structure for MoSCl.

Because the excitation width of our QCPMG pulse sequence is about 800 ppm, we are thus able to cover the whole known ^{95}Mo CS range using only one excitation offset. Because the resonance frequencies of our compounds were initially unknown, a first difficulty we encountered in the course of this work was localization of their signal in a time-saving way. Consequently, we initially used a single-pulse sequence in combination with MAS that enabled a wide excitation window. This approach was applied to $MoBr_2$ and $(Bu_4N)_2Mo_6Br_{14}$, and the corresponding spectra are sketched in Figure 2. Using the deduced offset information, we accumulated afterward the ^{95}Mo signals of the three octahedral cluster compounds using a QCPMG sequence. The QCPMG spectra acquired at 18.8 and 19.6 T are presented in Figures 3 and4.

The two spectra obtained for $Cs_2Mo_6Br_{14}$ can be easily explained on the basis of one crystallographic position, as shown by the two simulations presented in Figure 3a. The corresponding quadrupolar coupling and CS parameters are

dx.doi.org/10.1021/ic301648s | *Inorg. Chem.* 2013, 52, 617−627

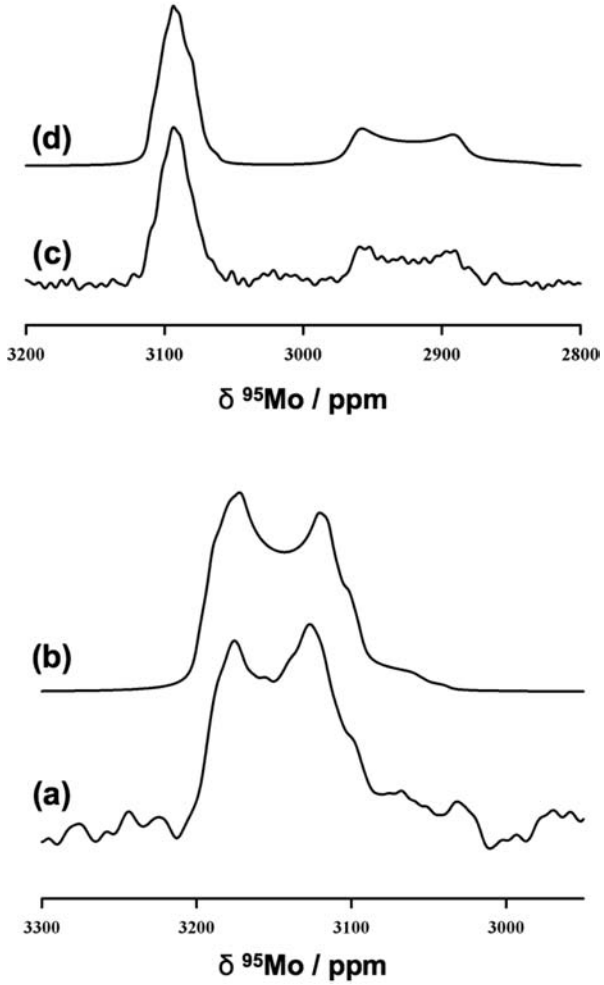

Figure 2. ^{95}Mo NMR spectra obtained at 18.8 T using a single-pulse sequence for $(Bu_4N)_2Mo_6Br_{14}$ (a) and the corresponding analytical simulation using the experimental parameters of Table 1 (b). ^{95}Mo NMR spectra obtained at 18.8 T using a single-pulse sequence for $MoBr_2$ (c) and the corresponding analytical simulation using the experimental parameters of Table 1 (d). 2784 and 2560 transients were acquired for $MoBr_2$ and $(Bu_4N)_2Mo_6Br_{14}$, respectively, with a repetition delay of 30 s in both cases.

reported in Table 1. The shape of the signal is clearly dominated by the second order quadrupolar coupling interaction, and no information about the CSA can be extracted. The absence of any visible distribution of signals shows that the statistical distribution in Cs atoms does not or only slightly influences the spectra. This is explained by the long Mo−Cs distances (4.744 Å for the shortest) and the weak interaction of Cs atoms with the clusters. The spectra of $(Bu_4N)_2Mo_6Br_{14}$ (see Figure 3b) were more difficult to acquire because this sample contains about 3 times less Mo atoms than $Cs_2Mo_6Br_{14}$. This entails a low resolution of the spectral line shape, which prevents any direct deconvolution. However, using the single-pulse spectrum sketched in Figure 2a and the three atomic sites occupied by molybdenum in the crystallographic structure of $(Bu_4N)_2Mo_6Br_{14}$, the NMR parameters can be roughly estimated. These parameters are shown in Table 1 and used in the two simulations of Figure 3b.

At this point, we can already get important information by comparing the spectra obtained for these two structurally similar compounds. Their experimental δ_{iso} values are comparable because they only differ by ∼40 ppm, which is quite low compared to the CS range of molybdenum. It is worth pointing out that this difference is also found between their computed isotropic chemical shielding values (see the Supporting Information). In contrast, C_Q of $(Bu_4N)_2Mo_6Br_{14}$ is significantly larger by ∼0.80 MHz experimentally and by ∼0.50 MHz from calculations (depending on the considered Mo atom). This seems to reveal a stronger influence of the chemical environment on C_Q than on δ_{iso}. This observation can be directly related to structural parameters. Variation of the calculated C_Q of an isolated $Mo_6Br_{14}^{2-}$ model cluster as a function of the Mo−Br^a distance has been studied (see the Supporting Information). Although only qualitative remarks can be drawn from this model, it is clear that a strong dependence exists between the C_Q parameter and the Mo−Br^a distance. The larger size of the countercation in $(Bu_4N)_2Mo_6Br_{14}$ involves a more diffuse positive charge inducing smaller experimental Mo−Br^a distances: 2.585 Å for Mo(2)−Br(7), 2.582 Å for Mo(1)−Br(5), and 2.579 Å for Mo(3)−Br(6) compared to 2.600 Å in $Cs_2Mo_6Br_{14}$. In light of our calculations, this explains the smaller C_Q of the Mo atoms in this latter compound. In contrast, the experimental Mo−Mo and Mo−Br^i bond lengths are not as much influenced by the nature of the countercations. Their average values are equal to 2.635 and 2.601 Å, respectively, in $Cs_2Mo_6Br_{14}$ and to 2.630 and 2.596 Å, respectively, in $(Bu_4N)_2Mo_6Br_{14}$.

The spectra of $MoBr_2$ shown in Figure 4 are different from the previous ones because they present two well-separated regions of signals. The right part, between +2900 and +3000 ppm, can be fairly modeled by a unique site. In contrast, because of its smaller width, the left part is more difficult to analyze. Indeed, this small width limits the gain for the sensitivity/resolution ratio that could be expected by using a QCPMG sequence, which is more efficient for large signals.[117,118] However, the single-pulse spectrum presented in Figure 2c can be best-fitted with two distinct signals, as required by the crystallographic structure. The corresponding NMR parameters are shown in Table 1. In $MoBr_2$, two types of Br^a atoms are present: the ones shared between different clusters [Br(4)] and the ones that lie between the cluster planes [Br(3)]. These latter Br atoms are subject to weak interactions, i.e., dispersion interactions with the closest plane. Consequently, the experimental Mo(1)−Br(3) bond length is 2.551 Å, compared to the Mo(2)−Br(4) and Mo(3)−Br(4) bond lengths, which are equal to 2.654 and 2.651 Å, respectively. Hence, on the basis of the discussion about the relationship between C_Q and the Mo−Br^a bond length (vide supra), we can confidently assign the large peak at low CS to Mo(1) that is linked to the nonshared Br^a. The narrow peak at high CS is the superimposition of the signals of Mo(2) and Mo(3) that are linked to shared Br^a. This assignation can be quantitatively confirmed by integration of the single-pulse spectrum presented in Figure 2c, as well as by our calculations of the C_Q parameters. Calculated σ_{iso} values also confirm this assignment. Indeed, the σ_{iso} values of Mo(2) and Mo(3) are almost equal, whereas the one of Mo(1) is computed to be ca. 120 ppm higher (see the Supporting Information). The average experimental Mo−Mo and Mo−Br^i bond lengths in one cluster of $MoBr_2$ are 2.631 and 2.598 Å, respectively, which are quite similar to the ones in $(Bu_4N)_2Mo_6Br_{14}$ and $Cs_2Mo_6Br_{14}$.

The QCPMG spectra obtained at 18.8 T for MoS_2Cl_3 and MoSCl are shown in Figure 5, and the one obtained for $Mo_3S_7Cl_4$ is shown in Figure 6. For these three compounds, to

dx.doi.org/10.1021/ic301648s | Inorg. Chem. 2013, 52, 617−627

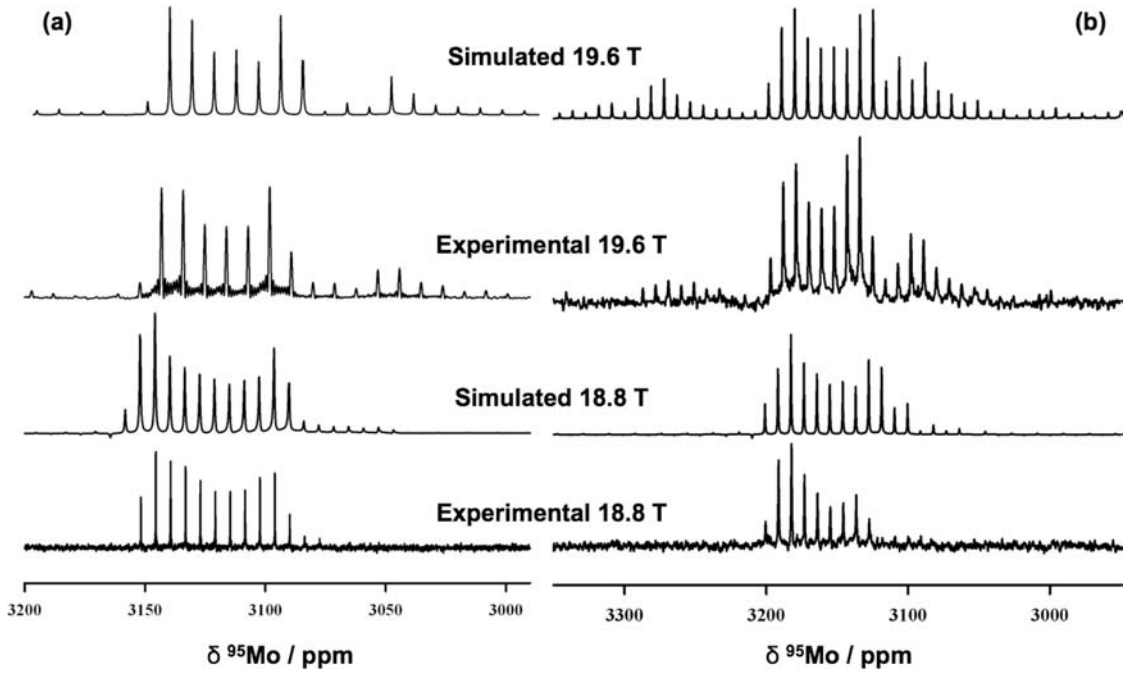

Figure 3. ^{95}Mo NMR spectra obtained at 18.8 T and at 19.6 T for $Cs_2Mo_6Br_{14}$ (a) and $(Bu_4N)_2Mo_6Br_{14}$ (b). The corresponding numerical simulations using the parameters shown in Table 1 are presented. 2048 (2560) and 4096 (4096) transients were acquired at 18.8 and 19.6 T, respectively, for $Cs_2Mo_6Br_{14}$ ($(Bu_4N)_2Mo_6Br_{14}$). A repetition delay of 30 s was applied at both magnetic fields for both compounds. 35 and 70 echoes were recorded per scan at 18.8 T for $Cs_2Mo_6Br_{14}$ and $(Bu_4N)_2Mo_6Br_{14}$, respectively, and 16 for both compounds at 19.6 T.

avoid the time-consuming accumulation of single-impulsion spectra, we adjusted our offset parameters based on our quantum-chemical calculations of the isotropic chemical shieldings. By comparison with the results obtained for the octahedral cluster compounds, we got in each case a good estimation of the signal position.

As seen in Figures 5a and 5c, the experimental spectra of MoS_2Cl_3 and MoSCl are both composed of only one peak in accordance with the only one crystallographically independent Mo atom in these structures. These two spectra do not present any clear discontinuity characteristic of the second-order quadrupolar coupling interaction. This absence can be attributed to the thinness of the signals, which, using a QCPMG pulse sequence, prevents us from getting well-resolved spectra. The same remark was previously made for the left peak of the $MoBr_2$ spectrum for which the small C_Q value limits the gain in resolution of the QCPMG pulse sequence. Furthermore, because we used the same pulse sequence for all of the studied compounds, it is also conceivable that the free induction decay is slightly truncated, making the normally sharp second-order quadrupolar coupling discontinuities smoother. Other explanations related to the nature of the sample can be considered, for example, the presence of minute quantities of paramagnetic impurities or the existence of dynamical processes in the compounds. We discarded the former possibility as MoS_2Cl_3 and MoSCl being synthesized in two different ways, using distinct nonmagnetic reagents, and our X-ray analysis does not evidence the presence of any impurity having a paramagnetic character. The latter possibility could occur in MoS_2Cl_3, although we have no evidence of such a process, but not in MoSCl, where the three-dimensional network prevents it. Thus, seeing the large uncertainty that we would obtain, we did not extract any accurate quadrupolar coupling parameters. However, for MoS_2Cl_3, on the basis of the calculated values presented in Table 1 and on the corresponding simulated spectrum of Figure 5b, C_Q probably lies between 3.5 and 4.0 MHz. It is worth pointing out that the inclusion of the CSA parameters in these simulations does not improve the agreement between theory and experiment (see the Supporting Information).

In accordance with its crystallographic structure, the spectrum of $Mo_3S_7Cl_4$ in Figure 6 shows three distinct isotropic signals. Like for MoS_2Cl_3 and MoSCl and probably for the same reasons, they do not display any second-order quadrupolar coupling line shape. In addition, in contrast to MoS_2Cl_3 and MoSCl, the signal is composed of spinning sidebands. If we focus on the isotropic part of the signal (see the inset of Figure 6), two high δ_{iso}, low C_Q signals and one low δ_{iso}, higher C_Q signals are observed. The computed σ_{iso} values for Mo(1), Mo(2), and Mo(3) are equal to −645, −989, and −953 ppm, respectively. Therefore, one can safely assign the peak at the lowest CS to Mo(1), which is also confirmed by its calculated C_Q value. Our calculations also suggest that the peaks at the highest and intermediate CS are due to Mo(2) and Mo(3), respectively. The presence of spinning sidebands in the spectrum of $Mo_3S_7Cl_4$ is due to a particularly large CSA. The anisotropic constants δ_{aniso} are calculated at 697, 1111, and 1076 ppm for Mo(1), Mo(2), and Mo(3), respectively. The computed values for Mo(2) and Mo(3) are larger than the largest CSA value ever experimentally observed for molybdenum, that is, 1010/1018 ppm (±5) in MoS_2.[91] Because the experimental data on $Mo_3S_7Cl_4$ do not allow us to confirm our calculated values, a more specific work would be required to accurately determine the CSA parameters of this compound. However, we provide in the Supporting Information a number of simulated spectra of $Mo_3S_7Cl_4$ that include both the CSA and quadrupolar coupling parameters. These data allow us to discuss the accuracy of our DFT-calculated parameters for the three Mo atoms of this compound and also to support our

dx.doi.org/10.1021/ic301648s | Inorg. Chem. 2013, 52, 617−627

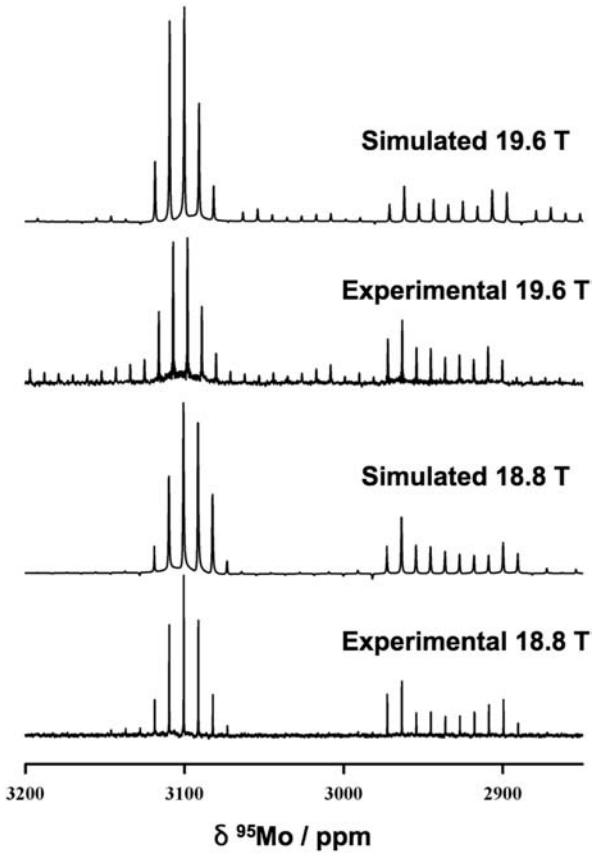

Figure 4. ^{95}Mo NMR spectra of $MoBr_2$ at 18.8 and 19.6 T. The corresponding numerical simulations using the parameters presented in Table 1 are presented. 2048 and 1024 transients were acquired at 18.8 and 19.6 T, respectively. A repetition delay of 30 s was applied at both magnetic fields. 70 and 16 echoes were recorded per scan at 18.8 and 19.6 T, respectively.

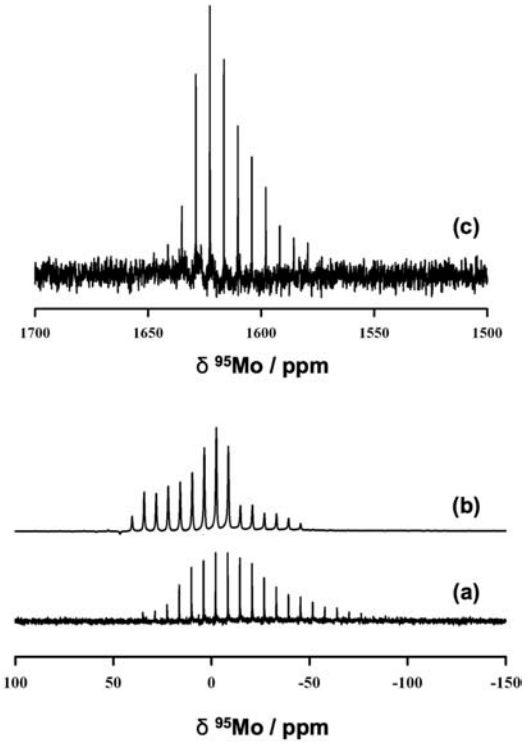

Figure 5. ^{95}Mo NMR spectrum obtained at 18.8 T for MoS_2Cl_3 (a) and the simulation obtained from the calculated parameters gathered in Table 1 (b). ^{95}Mo NMR spectrum obtained at 18.8 T for MoSCl (c). 800 and 443 transients were acquired for MoS_2Cl_3 and MoSCl, respectively. Repetition delays of 16 and 32 s were applied for MoS_2Cl_3 and MoSCl, respectively. 35 echoes were recorded per scan for each compound.

choice of not trying to extract the corresponding experimental parameters.

On the basis of the values gathered in Table 1, the relation we evidenced in the octahedral cluster compounds between the molybdenum C_Q and the bond lengths with their surrounding halogen ligands seems to be also valid for MoS_2Cl_3 and $Mo_3S_7Cl_4$. Indeed, in these compounds $\overline{d}_{Mo(2)-Cl}(Mo_3S_7Cl_4) \sim \overline{d}_{Mo(3)-Cl}(Mo_3S_7Cl_4) > \overline{d}_{Mo-Cl}(MoS_2Cl_3) > \overline{d}_{Mo(1)-Cl}(Mo_3S_7Cl_4)$, which corresponds to the inverse ordering of the calculated C_Q values. Similarly, MoSCl has the longest observed Mo−Cl distance and the smallest calculated C_Q parameter. However, because the arrangement of the S atoms

Table 1. Experimental ^{95}Mo Quadrupolar (C_Q^{exp}, η_Q^{exp}) and CS (δ_{iso}^{exp}) Parameters and Calculated Quadrupolar Parameters (C_Q^{calc} and η_Q^{calc}) for $MoBr_2$, $(Bu_4N)_2Mo_6Br_{14}$, $Cs_2Mo_6Br_{14}$, MoS_2Cl_3, $Mo_3S_7Cl_4$, and MoSCl (Experimental Uncertainties Given in Brackets; nd = Not Determined)

compound	atom	δ_{iso}^{exp} (ppm)	C_Q^{exp} (MHz)	C_Q^{calc} (MHz)	η_Q^{exp}	η_Q^{calc}
$(Bu_4N)_2Mo_6Br_{14}$[a]	Mo(1)	3204(5)	5.15 (0.20)	5.55	0.10 (0.20)	0.05
	Mo(2)	3203(5)	5.60 (0.20)	5.86	0.10 (0.20)	0.01
	Mo(3)	3218(5)	5.50 (0.20)	5.71	0.03 (0.20)	0.07
$Cs_2Mo_6Br_{14}$	Mo(1)	3166(3)	4.70 (0.10)	5.25	0.10 (0.10)	0.13
	Mo(1)	2985(3)	5.34 (0.10)	6.03	0.07 (0.20)	0.02
$MoBr_2$	Mo(2)[b]	3114(3)	2.83 (0.15)	3.24	0.34 (0.20)	0.18
	Mo(3)[b]	3104(3)	2.80 (0.15)	3.24	0.30 (0.20)	0.19
MoS_2Cl_3	Mo(1)	−18(5)	nd	3.86	nd	0.82
	Mo(1)	138(5)	nd	5.45	nd	0.15
$Mo_3S_7C_{l4}$	Mo(2)	253(5)	nd	2.35	nd	0.35
	Mo(3)	216(5)	nd	2.00	nd	0.29
MoSCl	Mo(1)	1618(5)	nd	0.92	nd	0.00

[a]Because of severe overlapping of the molybdenum signals in the case of $(Bu_4N)_2Mo_6Br_{14}$, a classical fitting procedure could not be carried out. NMR parameters were estimated both on the basis of the known crystal structure (three molybdenum sites) and on the basis of several simulations using GIPAW calculated values as a starting point. [b]The same remark is true for the Mo(2) and Mo(3) sites of $MoBr_2$.

dx.doi.org/10.1021/ic301648s | Inorg. Chem. 2013, 52, 617−627

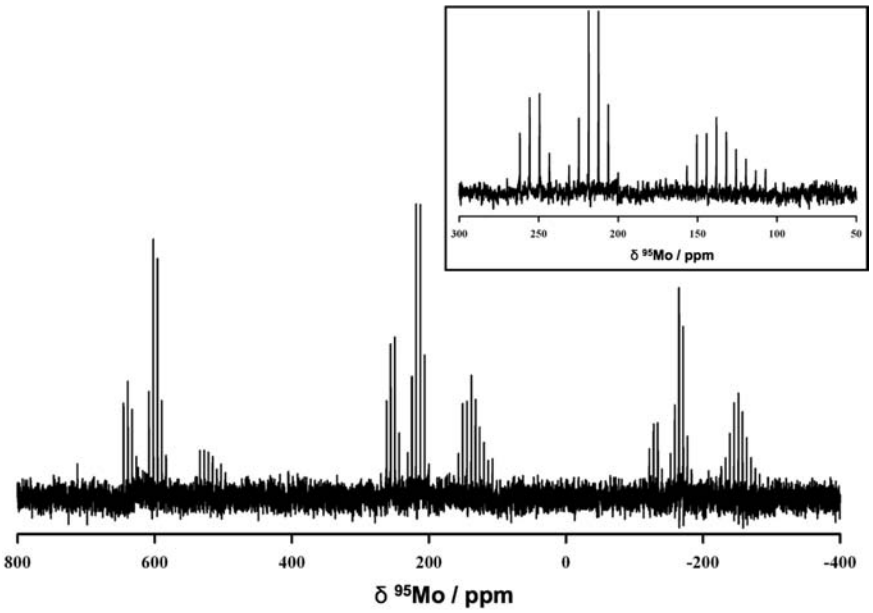

Figure 6. ^{95}Mo NMR spectrum obtained at 18.8 T for $Mo_3S_7Cl_4$. The inset presents a zoom on the isotropic part of the signal. 4882 transients were acquired with a repetition delay of 32 s. 35 echoes were recorded per scan.

is different in this compound, a direct comparison with MoS_2Cl_3 and $Mo_3S_7Cl_4$ is not possible.

The ^{95}Mo measurements presented above allow us to explore a large range of Mo oxidation degrees found in molybdenum cluster compounds: II+ for $MoBr_2$, $(Bu_4N)_2Mo_6Br_{14}$ and $Cs_2Mo_6Br_{14}$, III+ for MoSCl, IV+ for $Mo_3S_7Cl_4$, and V+ for MoS_2Cl_3. Only the oxidation degree I+ is not represented; Mo oxidation degrees 0 and VI+ do not exist in molybdenum cluster chemistry. Figure 7 sketches the correlation between the experimental δ_{iso} and calculated σ_{iso} values for the six studied compounds. Using a linear model, the correlation between the two sets of values is quite good with a coefficient of determination, R^2, of 0.99. The equation of the best linear fit is $\sigma_{iso} = -0.83\delta_{iso} - 758$, which leads to $\delta_{iso} = -1.20\sigma_{iso} - 913$. Considering the relationship between the CS and chemical shielding, the intercept of this latter equation can be assigned to σ_{iso} of the experimental reference, a 2.0 M aqueous solution of Na_2MoO_4. This quantity is not obvious to calculate because an isolated MoO_4^{2-} dianion neglects the fundamental influence of the solvent. An accurate calculation would require an explicit ensemble-averaging approach that is beyond the scope of this work. However, a good estimation can be obtained from the study of the solid-state Na_2MoO_4 compound. The ^{95}Mo σ_{iso} of this compound has been previously computed to be −816 ppm using an optimized structure, and its experimental δ_{iso} compared to aqueous Na_2MoO_4 is −33.5 ppm.[116] Consequently, the σ_{iso} value of aqueous Na_2MoO_4 is around −849.5 ppm. The difference between this value and the intercept of our best linear fit, −913 ppm, originates mainly because the slope of the linear fit deviates significantly from its ideal theoretical value, i.e., −1. Several previous theoretical studies have pointed out this deviation. For example, using the GIPAW approach, a similar behavior has been evidenced in the study of the ^{19}F,[119] ^{35}Cl,[120] ^{81}Br,[121] and ^{127}I nuclei.[122] Although these works focused on smaller CS ranges and on a single oxidation degree, a clear deviation from a −1 slope was systematically observed. Relativistic effects, in particular spin−orbit coupling, may be at the origin of this deviation in the case of bromine and iodine. However, it is rather unexpected that these effects significantly influence the calculation of ^{19}F and ^{35}Cl chemical shielding tensors. Furthermore, some of us previously showed that this influence is constant on the isotropic chemical shielding of molybdenum.[123] Therefore, this is probably not the missing ingredient in our calculations to explain the deviation of the slope. In contrast, it has been shown that a certain amount of Hartree−Fock exchange improves the slope of the linear fit for ^{57}Fe and ^{103}Rh isotropic CSs in organometallic compounds.[124] Because no implementation of the GIPAW approach in combination with the hybrid functional is available, we were not able to further evaluate such an influence.

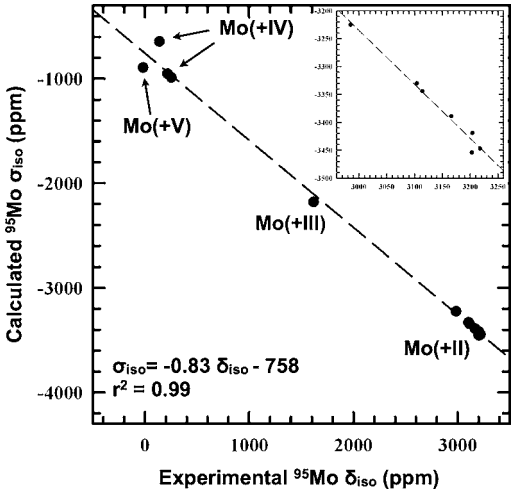

Figure 7. Experimental ^{95}Mo isotropic CS versus calculated ^{95}Mo isotropic chemical shielding for the six studied compounds (i.e., 12 distinct molybdenum sites). All calculated values were computed using optimized structures, and no referencing procedure was used. The dashed line corresponds to the equation of the best linear fit given in the left bottom corner. The inset is a focus in the region between 2960 and 3250 ppm.

dx.doi.org/10.1021/ic301648s | Inorg. Chem. 2013, 52, 617−627

The calculated value that deviates the most from the correlation corresponds to Mo(1) of $Mo_3S_7Cl_4$, which is also evidenced in the simulations presented in the Supporting Information. A possible explanation for this deviation is that, contrary to Mo(2) and Mo(3), Mo(1) is bound to two Cl atoms that interact through dispersion forces with the adjacent chain of clusters. With the dispersion interaction being not well described by GGA functionals, this could have a nonnegligible influence on the calculation of the chemical shielding of Mo(1). The same argument can be used to explain the weaker deviation for the Mo atom of MoS_2Cl_3. In this case, only one Cl atom is subjected to the dispersion interaction. Even if the deviation from the correlation for these few atoms is significant, about 100 ppm, this is a more than satisfactory result compared to the molybdenum CS range of ∼8000 ppm.

Overall, the fit equation compares well with the one obtained in our previous work.[116] In this study, the experimental CS range was restricted to −165.0 to +131.3 ppm and the equation obtained for the optimized structure of 12 molybdates was $\sigma_{iso} = -0.91\delta_{iso} - 826$. These results show the robustness of the GIPAW approach over a large CS range, about 3200 ppm. Up to now, this is the largest CS range that has been studied using this approach. Because the computational parameters were not tuned from one compound to another, in particular the pseudopotential of molybdenum remained unchanged for all calculations, this proves that this computational method can be used in a more general case for signal assignment or structure refinement. For this kind of application, in particular signal assignment, a high degree of accuracy is needed over a more restricted CS range. To show that we are able to access this level of precision, we focused on the CS range covered by the octahedral cluster compounds. As can be see in the inset of Figure 7, the correlation obtained for these three compounds, which represents seven signals, is very good ($R^2 = 0.97$) and the equation of the best linear fit is $\sigma_{iso} = -0.97\delta_{iso} - 332$.

CONCLUSIONS

We have demonstrated the relevance of ^{95}Mo SSNMR measurements of various molybdenum cluster compounds. To the best of our knowledge, this is the first time that such a study has been conducted for this class of materials. Our experiments were performed at 18.8 T, and also at 19.6 T for three compounds, using a QCPMG sequence under MAS conditions that allowed us to obtain spectra in a relatively short amount of experimental time. This has been achieved by specifically focusing our experiments on the central transition and the corresponding isotropic CS and quadrupolar coupling parameters. This is an important feature for further studies of more complex and diluted compounds, such as hybrid and nanomaterials, which are of more applicative interest.

For clusters of similar structure, our measurements have evidenced a clear relation between the C_Q parameter of a Mo atom and the corresponding bond lengths with its surrounding ligands. Furthermore, a correlation exists between the formal oxidation degree of a Mo atom in a given cluster and the corresponding δ_{iso}: the smaller the oxidation degree of a Mo atom, the higher the corresponding isotropic CS. These observations will be helpful for future experimental works on molybdenum cluster compounds. Indeed, because the excitation window of the QCPMG pulse sequence is narrow compared to the CS range of molybdenum, our results can be used to restrain the research window of a particular signal in the case where the Mo oxidation degree of the studied compound is known.

Because of the limited availability of the experimental facilities, it has not been possible to go more closely into the study of our compounds by accurately determining their CSA parameters. However, this should be made possible by using more specific experimental equipments (static or large-volume probes) to perform static experiments under several magnetic fields. In the case of very broad signals, such as the one of $Mo_3S_7Cl_4$, wide-bandwidth pulse sequences such as WURST-QCPMG could be performed.[125−127] In the particular case of $(Bu_4N)_2Mo_6Br_{14}$, cross-polarization ^{1}H−^{95}Mo experiments would also be useful to overcome the low sensitivity of the sample.

Finally, the present study has shown that the PAW and GIPAW approaches can be applied to the study of molybdenum cluster compounds where metal−metal bonds occur. Our work has evidenced the robustness of these computational approaches over a large molybdenum CS range, about 3200 ppm, because similar computational parameters have been used for all of the different oxidation degrees of Mo. The observed correlation between calculated isotropic shielding and experimental isotropic CS values is good and is quite similar to previous work on fully oxidized molybdenum systems. We are confident that this work will motivate new and original studies on molybdenum cluster compounds.

ASSOCIATED CONTENT

Supporting Information

Various pulse sequences used in this work as well as the pseudopotential definitions, the Monkhorst−Pack *k*-point grid densities used for geometry optimization, calculations of the corresponding NMR parameters and computational parameters used to perform geometry optimization, calculated isotropic chemical shielding obtained from the geometry-optimized structures of the six studied molybdenum cluster compounds, correlation that exists between the Mo−Br[a] bond length and the corresponding C_Q parameter in an idealized isolated $Mo_6Br_{14}^{2-}$ cluster, and simulated spectra of MoS_2Cl_3 and $Mo_3S_7Cl_4$ using various sets of CSA and quadrupolar coupling parameters. This material is available free of charge via the Internet at http://pubs.acs.org.

AUTHOR INFORMATION

Corresponding Author

*E-mail: cuny.jerome@phys.chem.ethz.ch (J.C.), laurent.delevoye@ensc-lille.fr (L.D.), regis.gautier@ensc-rennes.fr (R.G.).

Present Address

‡Department of Chemistry and Applied Biosciences, ETH Zurich, and Facoltà di Informatica, Istituto di Scienze Computazionali, Università della Svizzera Italiana, Via G. Buffi 13, 6900 Lugano, Switzerland.

Notes

The authors declare no competing financial interest.

ACKNOWLEDGMENTS

R.G. and L.L.P. are indebted to the Région Bretagne for a Ph.D. grant (to J.C.). This work was granted access to the HPC resources of CINES under allocation 2010-[scr6170] made by GENCI (Grand Equipement National de Calcul Intensif).

Financial support from the TGE RMN THC Fr 3050 for conducting the research is gratefully acknowledged. The authors acknowledge support of the French Agence Nationale de la Recherche (ANR) under Grant NMRTHEO (ANR-09-JCJC-0088-01). The National High Magnetic Field Laboratory is supported by the National Science Foundation and the State of Florida through Cooperative Agreement DMR-0084173.

REFERENCES

(1) Cotton, F. A. *Inorg. Chem.* **1964**, *3*, 1217−1220.
(2) Maverick, A. W.; Harry, H. B. *J. Am. Chem. Soc.* **1981**, *103*, 1298−1300.
(3) Converse, J. G.; McCarley, R. E. *Inorg. Chem.* **1970**, *9*, 1361−1366.
(4) Peric, B.; Cordier, S.; Cuny, J.; Gautier, R.; Guizouarn, T.; Planinic, P. *Chem.—Eur. J.* **2011**, *17*, 6263−6271.
(5) Saito, T.; Imoto, H. *Bull. Soc. Chim. Jpn.* **1996**, *69*, 2403.
(6) Simon, A. In *Clusters and Colloids—From Theory to Application*; Schmidt, G., Ed.; Verlag Chemie: Weinheim, 1994; pp 373−458.
(7) Perrin, C. *J. Alloys Compd.* **1997**, *263−263*, 10.
(8) Barrier, N.; Fontaine, B.; Pierrefixe, S.; Gautier, R.; Gougeon, P. *Inorg. Chem.* **2009**, *48*, 3848−3856.
(9) Potel, M.; Chevrel, R.; Sergent, M. *J. Solid State Chem.* **1980**, *35*, 286.
(10) Murugan, P.; Kumar, V.; Kawazoe, Y.; Otta, N. *Appl. Phys. Lett.* **2008**, *92*, 203112.
(11) Llusar, R.; Vicent, C. *Coord. Chem. Rev.* **2010**, *254*, 1534−1548.
(12) Shestopalov, M. A.; Ledneva, A.; Cordier, S.; Hernandez, O.; Potel, M.; Roisnel, T.; Naumov, N. G.; Perrin, C. *Angew. Chem.* **2011**, *50*, 7300.
(13) Cario, L.; Vaju, C.; Corraze, B.; Guiot, V.; Janod, E. *Adv. Mater.* **2010**, *22*, 5193.
(14) Nocera, D. G.; Gray, H. B. *J. Am. Chem. Soc.* **1984**, *106*, 824.
(15) Chevrel, R.; Sergent, M.; Prigent, J. *J. Solid State Chem.* **1971**, *3*, 515−519.
(16) Perrin, C.; Sergent, M. *J. Chem. Res. (S)* **1983**, 38−39.
(17) Remškar, M.; Mrzel, A.; Viršek, M.; Jesih, A. *Adv. Mater.* **2007**, *19*, 4276−4278.
(18) Domenici, V.; Conradi, M.; Remškar, M.; Viršek, M.; Zupančič, B.; Mrzel, A.; Chambers, M.; Zalar, B. *J. Mater. Sci.* **2011**, *46*, 3639−3645.
(19) Vrbanic, D.; Remskar, M.; Jesih, A.; Mrzel, A.; Umek, P.; Ponikvar, M.; Jancar, B.; Meden, A.; Novosel, B.; Pejovnik, S.; Venturini, P.; Coleman, J. C.; Mihailovic, D. *Nanotechnology* **2004**, *15*, 635.
(20) Mihailovic, D. *Prog. Mater. Sci.* **2009**, *54*, 309−350.
(21) Joly-Pottuz, L.; Dassenoy, F.; Martin, J.; Vrbanic, D.; Mrzel, A.; Mihailovic, D.; Vogel, W.; Montagnac, G. *Tribol. Lett.* **2005**, *18*, 385−393.
(22) Doyle, J. J.; Nicolosi, V.; O'Flaherty, S. M.; Vengust, D.; Drury, A.; Mihailovic, D.; Coleman, J. N.; Blau, W. J. *Chem. Phys. Lett.* **2007**, *435*, 109−113.
(23) Vengust, D.; Pfuner, F.; Degiorgi, L.; Vilfan, I.; Nicolosi, V.; Coleman, J. N.; Mihailovic, D. *Phys. Rev. B: Condens. Matter Mater. Phys.* **2007**, *76*, 075106.
(24) Dassenoy, F.; Joly-Pottuz, L.; Martin, J.; Vrbanic, D.; Mrzel, A.; Mihailovic, D.; Vogel, W.; Montagnac, G. *J. Eur. Ceram. Soc.* **2007**, *27*, 915−919.
(25) Nicolosi, V.; Vrbanic, D.; Mrzel, A.; McCauley, J.; O'Flaherty, S.; McGuinness, C.; Compagnini, G.; Mihailovic, D.; Blau, W. J.; Coleman, J. N. *J. Phys. Chem. B* **2005**, *109*, 7124−7133.
(26) Nicolosi, V.; Vrbanic, D.; Mrzel, A.; McCauley, J.; O'Flaherty, S.; Mihailovic, D.; Blau, W. J.; Coleman, J. N. *Chem. Phys. Lett.* **2005**, *401*, 13−18.
(27) McCarthy, D. N.; Nicolosi, V.; Vengust, D.; Mihailovic, D.; Compagnini, G.; Blau, W. J.; Coleman, J. N. *J. Appl. Phys.* **2007**, *101*, 014317.
(28) Zhou, T.; Lenoir, B.; Colin, M.; Dauscher, A.; Al Rahal Al Orabi, R.; Gougeon, P.; Potel, M.; Guilmeau, E. *Appl. Phys. Lett.* **2011**, *98*, 162106.
(29) Potel, M.; Chevrel, R.; Sergent, M. *Acta Crystallogr., Sect. B: Struct. Sci.* **1980**, *36*, 1545−1548.
(30) Cordier, S.; Kirakci, K.; Méry, D.; Perrin, C.; Astruc, D. *Inorg. Chem. Acta* **2006**, *359*, 1705.
(31) Grasset, F.; Dorson, F.; Cordier, S.; Molard, Y.; Perrin, C.; Marie, A.-M.; Sasaki, T.; Haneda, H.; Bando, Y.; Mortier, M. *Adv. Mater.* **2008**, *20*, 143−148.
(32) Dechézelles, F.; Aubert, T.; Grasset, F.; Cordier, S.; Barthou, C.; Schwob, C.; Maître, A.; Vallée, R. A. L.; Cramail, H.; Ravaine, S. *Phys. Chem. Chem. Phys.* **2010**, *12*, 11993−11999.
(33) Gosh, R. N.; Baker, G. L.; Ruud, C.; Nocera, D. G. *Appl. Phys. Lett.* **1999**, *75*, 19.
(34) Gosh, R. N.; Askeland, P. A.; Kramer, S.; Loloee, R. *Appl. Phys. Lett.* **2011**, *98*, 221103.
(35) Grasset, F.; Molard, Y.; Cordier, S.; Dorson, F.; Mortier, M.; Perrin, C.; Guilloux-Viry, M.; Sasaki, T.; Haneda, H. *Adv. Mater.* **2008**, *20*, 1710−1715.
(36) Dybtsef, D.; Serre, C.; Schmitz, B.; Hirscher, M.; Latroche, M.; Llewellyn, P.; Cordier, S.; Molard, Y.; Haouas, M.; Taulelle, F.; Férey, G. *Langmuir* **2010**, *26*, 11283.
(37) Gorman, C. B.; Su, W. Y.; Jiang, H.; Watson, C. M.; Boyle, P. *Chem. Commun.* **1999**, 877−878.
(38) Méry, D.; Plault, L.; Nlate, S.; Astruc, D.; Cordier, S.; Kirakci, K.; Perrin, C. *Z. Anorg. Allg. Chem.* **2005**, *631*, 2746.
(39) Mery, D.; Ornelas, C.; Daniel, M.-C.; Ruiz, J.; Rodrigues, J.; Astruc, D.; Cordier, S.; Kirakci, K.; Perrin, C. *C. R. Chim.* **2005**, *8*, 1789.
(40) Saito, M.; Nishida, T.; Yamagata, T.; Yamagata, Y.; Yamaguchi, Y. *Inorg. Chem.* **1986**, *25*, 1111−1117.
(41) Szczepura, L. F.; Ketcham, K. A.; Ooro, B. A.; Edwards, J. A.; Templeton, J. N.; Cedeño, D. L.; Jircitano, A. J. *Inorg. Chem.* **2008**, *47*, 7271−7278.
(42) Perruchas, S.; Flores, S.; Jousselme, B.; Lobkovsky, E.; Abruna, H.; DiSalvo, F. J. *Inorg. Chem.* **2007**, *46*, 8976.
(43) Prabusankar, G.; Molard, Y.; Cordier, S.; Golhen, S.; Le Gal, Y.; Perrin, C.; Kahlal, S.; Halet, J.-F.; Ouahab, L. *Eur. J. Inorg. Chem.* **2009**, *14*, 2153−2161.
(44) Golden, J. H.; Deng, H. B.; Disalvo, F. J.; Fréchet, J. M. J.; Thompson, P. M. *Science* **1995**, *268*, 1463.
(45) Molard, Y.; Dorson, F.; Circu, V.; Roisnel, T.; Artzner, F.; Cordier, S. *Angew. Chem., Int. Ed.* **2010**, *49*, 3351−3355.
(46) Mocanu, A. S.; Amela-Cortes, M.; Molard, Y.; Circu, V.; Cordier, S. *Chem. Commun.* **2011**, *47*, 2056.
(47) Davidson, P.; Batail, P.; Sanchez, C. *Prog. Polym. Sci.* **1997**, *22*, 913.
(48) Ababou-Girard, S.; Cordier, S.; Fabre, B.; Molard, Y.; Perrin, C. *ChemPhysChem* **2007**, *8*, 2086−2090.
(49) Fabre, B.; Cordier, S.; Ababou-Girard, S.; Molard, Y.; Perrin, C.; Godet, C. *J. Phys. Chem. C* **2009**, *113*, 17437.
(50) Ooms, K. J.; Wasylishen, R. E. *J. Am. Chem. Soc.* **2004**, *126*, 10972−10980.
(51) Rossini, A. J.; Schurko, R. W. *J. Am. Chem. Soc.* **2006**, *128*, 10391−10402.
(52) Ooms, K. J.; Feindel, K. W.; Willans, M. J.; Wasylishen, R. E.; Hanna, J. V.; Pike, K. J.; Smith, M. E. *Solid State Nucl. Magn. Reson.* **2005**, *28*, 125−134.
(53) Willans, M. J.; Feindel, K. W.; Ooms, K. J.; Wasylishen, R. E. *Chem.—Eur. J.* **2006**, *12*, 159−168.
(54) Tang, J. A.; Ellis, B. D.; Warren, T. H.; Hanna, J. V.; Macdonald, C. L. B.; Schurko, R. W. *J. Am. Chem. Soc.* **2007**, *129*, 13049−13065.
(55) MacKenzie, K. J. D.; Smith, M. E. *Multinuclear Solid-State NMR of Inorganic Materials*; Pergamon: New York, 2002.
(56) Lynch, G. F.; Segel, S. L. *Can. J. Phys.* **1972**, *50*, 567−572.
(57) Machida, N.; Eckert, H. *Solid State Ionics* **1998**, *107*, 255−268.
(58) Han, O. H.; Lin, C. Y.; Haller, G. L. *Catal. Lett.* **1992**, *14*, 1−9.

(59) Han, O. H.; Lin, C. Y.; Sustache, N.; McMillan, M.; Carruthers, J. D.; Zilm, K. W.; Haller, G. L. *Appl. Catal., A* **1993**, *98*, 195−210.
(60) Santagneli, S. H.; de Araujo, C. C.; Strojek, W.; Eckert, H.; Poirier, G.; Ribeiro, S. J. L.; Messaddeq, Y. *J. Phys. Chem. B* **2007**, *111*, 10109−10117.
(61) Zheng, H.; Ma, D.; Bao, X.; Hu, J. Z.; Kwak, J. H.; Wang, Y.; Peden, C. H. F. *J. Am. Chem. Soc.* **2008**, *130*, 3722−3723.
(62) Hu, J. Z.; Kwak, J. H.; Wang, Y.; Peden, C. H. F.; Zheng, H.; Ma, D.; Bao, X. *J. Phys. Chem. C* **2009**, *113*, 2936−2942.
(63) Kroeker, S.; Farnan, I.; Schuller, S.; Advocat, T. *Mater. Res. Soc. Symp. Proc.* **2009**, 1124.
(64) Panich, A. M.; Shames, A. I.; Rosentsveig, R.; Tenne, R. *J. Phys.: Condens. Matter* **2009**, *21*, 395301.
(65) Magnin, M.; Schuller, S.; Mercier, C.; Trébosc, J.; Caurant, D.; Majérus, O.; Angéli, F.; Charpentier, T. *J. Am. Ceram. Soc.* **2011**, *94*, 4274−4282.
(66) Edwards, J. C.; Adams, R. D.; Ellis, P. D. *J. Am. Chem. Soc.* **1990**, *112*, 8349−8364.
(67) Edwards, J. C.; Ellis, P. D. *Langmuir* **1991**, *7*, 2117−2134.
(68) Eichele, K.; Wasylishen, R. E.; Nelson, J. H. *J. Phys. Chem. A* **1997**, *101*, 5463−5468.
(69) Vosegaard, T.; Skibsted, J.; Jakobsen, H. *J. Phys. Chem. A* **1999**, *103*, 9144−9149.
(70) Bryce, D. L.; Wasylishen, R. E. *Phys. Chem. Chem. Phys.* **2002**, *4*, 3591−3600.
(71) Forgeron, M. A. M.; Wasylishen, R. E. *J. Am. Chem. Soc.* **2006**, *128*, 7817−7827.
(72) Forgeron, M. A. M.; Wasylishen, R. E. *Phys. Chem. Chem. Phys.* **2008**, *10*, 574−581.
(73) Iijima, T.; Yamase, T.; Tansho, M.; Shimizu, T.; Nishimura, K. *Chem. Phys. Lett.* **2010**, *487*, 232−236.
(74) Edwards, J. C.; Ellis, P. D. *Magn. Reson. Chem.* **1990**, *28*, S59−S67.
(75) Kault, W. D.; Krueger, H.; Lutz, O.; Maier, H.; Nolle, A. *Z. Naturforsch., A: Phys. Sci.* **1976**, *31*, 351−356.
(76) Nolle, A. *Z. Phys. A: At. Nucl.* **1977**, *280*, 231−234.
(77) Cordischi, D. V. M.; Gazzoli, D. *Gazz. Chim. Ital.* **1983**, *113*, 579−585.
(78) Aleksashin, B.; Verkhovskii, S.; Mikhalyov, K.; Arkhipov, V.; Goshchitskii, B.; Stepanov, A. *Solid State Commun.* **1985**, *56*, 209−213.
(79) Mastikhin, V.; Lapina, O.; Maximovskaya, R. *Chem. Phys. Lett.* **1988**, *148*, 413−416.
(80) Edwards, J. C.; Zubieta, J.; Shaikh, S. N.; Chen, Q.; Bank, S.; Ellis, P. D. *Inorg. Chem.* **1990**, *29*, 3381−3393.
(81) Edwards, J. C.; Ellis, P. D. *Magn. Reson. Chem.* **1990**, *28*, S59−S67.
(82) Stringfellow, T. C.; Wu, G.; Wasylishen, R. E. *J. Phys. Chem. B* **1997**, *101*, 9651−9656.
(83) Bastow, T. J. *Solid State Nucl. Magn. Reson.* **2003**, *23*, 116−118.
(84) Bastow, T. J. *Solid State Nucl. Magn. Reson.* **1998**, *12*, 191−199.
(85) Hamard, C.; Peña, O.; Le Floch, M. *Solid State Commun.* **2000**, *113*, 489−494.
(86) Le Pollès, L.; Gautier, R.; Ameline, J. C.; Le Floch, M.; Peña, O. *Solid State Commun.* **2003**, *125*, 597−600.
(87) Mark, E. S. *Annu. Rep. NMR Spectrosc.* **2001**, *Volume 43*, 121−175.
(88) d'Espinose de Lacaillerie, J.-B.; Barberon, F.; Romanenko, K. V.; Lapina, O. B.; Le Pollès, L.; Gautier, R.; Gan, Z. *J. Phys. Chem. B* **2005**, *109*, 14033−14042.
(89) Hove, A. R.; Bildsœ, H.; Skibsted, J.; Brorson, M.; Jakobsen, H. J. *Inorg. Chem.* **2006**, *45*, 10873−10881.
(90) d'Espinose de Lacaillerie, J.-B.; Gan, Z. *Appl. Magn. Reson.* **2007**, *32*, 499−511.
(91) Jakobsen, H. J.; Bildse, H.; Skibsted, J.; Brorson, M.; Schaumburg, K. *Chem. Commun.* **2010**, *46*, 2103−2105.
(92) Malito, J. *J. Ann. Rep. NMR Spectrosc.* **1997**, *33*, 151.
(93) Kaupp, M.; Bühl, M.; Malkin, V. G. *Calculation of NMR and EPR Parameters: Theory and Applications*; Wiley-VCH: New York, 2004.
(94) Mauri, F.; Pfrommer, B. G.; Louie, S. G. *Phys. Rev. Lett.* **1996**, *77*, 5300−5303.
(95) Sebastiani, D.; Parrinello, M. *J. Phys. Chem. A* **2001**, *105*, 1951−1958.
(96) Thonhauser, T.; Ceresoli, D.; Mostofi, A. A.; Marzari, N.; Resta, R.; Vanderbilt, D. *J. Chem. Phys.* **2009**, *131*, 101101−4.
(97) Pickard, C. J.; Mauri, F. *Phys. Rev. B: Condens. Matter Mater. Phys.* **2001**, *63*, 245101.
(98) Petrilli, H. M.; Blöchl, P. E.; Blaha, P.; Schwarz, K. *Phys. Rev. B: Condens. Matter Mater. Phys.* **1998**, *57*, 14690−14697.
(99) Charpentier, T. *Solid State Nucl. Magn. Reson.* **2011**, *40*, 1−20.
(100) Zheng, Y.-Q.; Grin, Y.; von Schnering, H. G. *Z. Kristallogr.-New Cryst. Struct.* **1998**, *213*, 469−470.
(101) Kirakci, K.; Cordier, S.; Roisnel, T.; Golhen, S.; Perrin, C. *Z. Kristallogr.* **2005**, *220*, 116−118.
(102) Kirakci, K.; Cordier, S.; Perrin, C. *Z. Anorg. Allg. Chem.* **2005**, *631*, 411−416.
(103) Marcoll, J.; Rabenau, A.; Mootz, D.; Wunderlich, H. *Rev. Chim. Miner.* **1974**, *11*, 607−615.
(104) Perrin, C.; Chevrel, R.; Sergent, M. *C. R. Acad. Sci. Paris* **1975**, *t. 280*, 949−950.
(105) Larsen, F. H.; Jakobsen, H. J.; Ellis, P. D.; Nielsen, N. C. *J. Phys. Chem. A* **1997**, *101*, 8597−8606.
(106) Larsen, F. H.; Jakobsen, H. J.; Ellis, P. D.; Nielsen, N. C. *J. Magn. Reson.* **1998**, *131*, 144−147.
(107) Larsen, F. H.; Skibsted, J.; Jakobsen, H. J.; Nielsen, N. C. *J. Am. Chem. Soc.* **2000**, *122*, 7080−7086.
(108) Bak, M.; Rasmussen, J. T.; Nielsen, N. C. *J. Magn. Reson.* **2000**, *147*, 296−330.
(109) Massiot, D.; Fayon, F.; Capron, M.; King, I.; Calv, S. L.; Alonso, B.; Durand, J.-O.; Bujoli, B.; Gan, Z.; Hoatson, G. *Magn. Reson. Chem.* **2002**, *40*, 70−76.
(110) Segall, M. D.; Lindan, P. J. D.; Probert, M. J.; Pickard, C. J.; Hasnip, P. J.; Clark, S. J.; Payne, M. C. *J. Phys.: Condens. Matter* **2002**, *14*, 2717−2744.
(111) Perdew, J. P.; Burke, K.; Ernzerhof, M. *Phys. Rev. Lett.* **1996**, *77*, 3865−3868.
(112) Yates, J. R.; Pickard, C. J.; Mauri, F. *Phys. Rev. B: Condens. Matter Mater. Phys.* **2007**, *76*, 024401.
(113) Blöchl, P. E. *Phys. Rev. B: Condens. Matter Mater. Phys.* **1994**, *50*, 17953−17979.
(114) Monkhorst, H. J.; Pack, J. D. *Phys. Rev. B: Condens. Matter Mater. Phys.* **1976**, *13*, 5188−5192.
(115) Pyykkö, P. *Mol. Phys.* **2001**, *99*, 1617−1629.
(116) Cuny, J.; Furet, E.; Gautier, R.; Le Pollès, L.; Pickard, C. J.; d'Espinose de Lacaillerie, J.-B. *ChemPhysChem* **2009**, *10*, 3320−3329.
(117) Sutrisno, A.; Lu, C.; Lipson, R. H.; Huang, Y. *J. Phys. Chem. C* **2009**, *113*, 21196−21201.
(118) Hamaed, H.; Laschuk, M. W.; Terskikh, V. V.; Schurko, R. W. *J. Am. Chem. Soc.* **2009**, *131*, 8271−8279.
(119) Sadoc, A.; Body, M.; Legein, C.; Biswal, M.; Fayon, F.; Rocquefelte, X.; Boucher, F. *Phys. Chem. Chem. Phys.* **2011**, *13*, 18539−18550.
(120) Chapman, R. P.; Bryce, D. L. *Phys. Chem. Chem. Phys.* **2009**, *11*, 6987−6998.
(121) Widdifield, C. M.; Bryce, D. L. *J. Phys. Chem. A* **2010**, *114*, 2102−2116.
(122) Widdifield, C. M.; Bryce, D. L. *J. Phys. Chem. A* **2010**, *114*, 2102−2116.
(123) Cuny, J.; Sykina, K.; Fontaine, B.; Le Pollès, L.; Pickard, C. J.; Gautier, R. *Phys. Chem. Chem. Phys.* **2011**, *13*, 19471−19479.
(124) Bühl, M. *Chem. Phys. Lett.* **1997**, *267*, 251−257.
(125) O'Dell, L. A.; Schurko, R. W. *Chem. Phys. Lett.* **2008**, *464*, 97−102.
(126) Tang, J. A.; O'Dell, L. A.; Aguiar, P. M.; Lucier, B. E.; Sakellariou, D.; Schurko, R. W. *Chem. Phys. Lett.* **2008**, *466*, 227−234.
(127) O'Dell, L. A.; Rossini, A. J.; Schurko, R. W. *Chem. Phys. Lett.* **2009**, *468*, 330−335.